Electrodeposition of a Pd-Ni/TiO2 Composite Coating on 316L SS and Its Corrosion Behavior in Hot Sulfuric Acid Solution

Zhiheng Zhang, Junlei Tang, Yingying Wang, Hu Wang, Bernard Normand, Yu Zuo

coatings

MDPI

Article

Electrodeposition of a Pd-Ni/TiO_2 Composite Coating on 316L SS and Its Corrosion Behavior in Hot Sulfuric Acid Solution

Zhiheng Zhang [1], Junlei Tang [1,*], Yingying Wang [1], Hu Wang [2], Bernard Normand [3,*] and Yu Zuo [4]

1 School of Chemistry and Chemical Engineering, Southwest Petroleum University, Chengdu 610500, China; zhangzhtony@126.com (Z.Z.); yingyingwanglyon@126.com (Y.W.)
2 School of Material Science and Engineering, Southwest Petroleum University, Chengdu 610500, China; senty78@126.com
3 MATEIS UMR CNRS 5510, Universitéde Lyon, INSA-Lyon, Bat L. de Vinci, 21 Avenue Jean Capelle, 69621 Villeurbanne Cedex, France
4 School of Material Science and Engineering, Beijing University of Chemical Technology, Beijing 100029, China; zuoy@mail.buct.edu.cn
* Correspondence: tangjunlei@126.com (J.T.); bernard.normand@insa-lyon.fr (B.N.); Tel.: +86-28-8303-7361 (J.T.)

Received: 2 April 2018; Accepted: 3 May 2018; Published: 11 May 2018

Abstract: Pd-Ni/TiO_2 composite coatings were elaborated on 316L stainless steel by an electrodeposition method. The specimens were obtained from an electrolytic bath that contained various contents (5, 10, and 15 g L^{-1}) of nanosized TiO_2 particles. X-ray diffraction (XRD) characterization showed that increasing the TiO_2 content in the coatings can decrease the crystal grain size. The surface morphology and chemical composition of the composite coatings were modified by the addition of TiO_2 particles in the electrolyte, as shown by scanning electron microscopy (SEM) and energy dispersive spectrometry (EDS) methods, respectively. The TiO_2 content also significantly affected the mechanical and electrochemical properties of the Pd-Ni/TiO_2 composite coatings. The microhardness of the Pd-Ni/TiO_2 composite coatings can be enhanced by increasing the TiO_2 content in the coatings. With the addition of 5 g L^{-1} TiO_2 particles to the electrolyte, the deposited Pd-Ni/TiO_2 composite coating presented a remarkably increased corrosion resistance when exposed to a sulfuric acid solution at 60 °C compared with that of the Pd-Ni alloy coating. Nevertheless, the further addition of TiO_2 particles into the electrolytic bath did not further improve the corrosion resistance of the composite coating.

Keywords: Pd-Ni/TiO_2; electrodeposition; composite coating; corrosion

1. Introduction

Currently, stainless steel is commonly used in various applications because of its favorable corrosion resistance. However, in some industries, such as the synthetic fiber industry, waste heat recovery, and alternative energies (i.e., proton exchange membrane (PEM) fuel cells and hydrogen production by water electrolysis), stainless steel is prone to corrosion in hot dilute sulfuric acid. Because the passivation of stainless steel is not stable and corrosion resistance decreases corrosion occurs in acidic media [1]. Therefore, different techniques are used to elaborate coatings on stainless steel, such as chromium nitride coatings on stainless steel for conductive components using physical vapor deposition (PVD) [2] and superior tribological properties, corrosion resistance and biocompatibility of titanium-amorphous carbon-coated 316L stainless steel (SS) through magnetron

sputtering [3], etc. However, these techniques cannot be applied to large-scale or special-shape workpieces, and several methods are not economical due to their intensive energy consumption. Hence, the wide-scale use of these techniques in various industries is limited.

Electrodeposition is a conventional technique to obtain thin coatings to modify stainless steel surface. Palladium [1,4,5] and its alloys, such as Pd-Co [6], Pd-Cr [7], Pd-Ni/Pd-Cu [8], and Pd-Ni-W [9] have modified surface of stainless steel by electroplating or electroless plating on stainless steel to obtain excellent corrosion resistance in hot sulfuric acid solutions or acetic and formic acid mixtures. Because Pd-based coating increases galvanic potential of coated stainless steel, galvanic coupling can be advantageously used to promote passivation of stainless steel in corrosive media [4]. Because of the existence of insoluble particles (TiO_2 [10], Al_2O_3 [11], SiC [12], ZrO_2 [13], etc.) in the metallic matrix, composite coatings often have better corrosion resistance and higher wear resistance compared with metallic coatings. Electrodeposition also is a convenient technique that is used to obtain ideal composite coatings by adjusting the deposition parameters and operating conditions [14]. Zn-Ni/TiO_2 [15], Ni-W/TiO_2 [16], Ni-Cr/TiO_2 [17] and other types of composite coatings have been identified as having a higher corrosion resistance regarding alloy coatings.

Furthermore, the corrosion resistance of protective coatings in various industries is required, and several other characteristics, such as contact resistance and mechanical properties in certain circumstances (i.e., bipolar plates in PEM fuel cells and electronic components), are needed as well. Take the electrolyte in PEM fuel cell as an example: it is mainly composed of 5–20 wt.% H_2SO_4 solution working at 60–80 °C. Because Pd-Ni alloy coatings have been less investigated as a matrix of composite coating, this paper deals with the opportunity to combine high corrosion resistance developed previously and its excellent contact resistance [18,19], with TiO_2 often used for improving wear resistance of composite coatings [16,20,21]. Thus, Pd-Ni/TiO_2 composite materials might be a promising protective coating for various stainless steels exposed to corrosive hot dilute sulfuric acid in several industrial fields (chemistry, energy, etc.)

Generally, pulse current (PC) deposition can provide composite coatings with a refined deposit in comparison with direct current (DC) deposition. Moreover, the pulse electrodeposition process offers an accelerated nucleation rate and a modified morphology during composite coating fabrication [22].

Based on the observations above, this research focused on the investigation of Pd-Ni/TiO_2 composite coatings on 316L stainless steel with various contents of nanosized TiO_2 particles by electrodeposition. The corrosion resistance of 316L stainless steel in hot dilute sulfuric acid was significantly improved by both electrochemical modification and the barrier effects of the Pd-Ni/TiO_2 composite coating. Additionally, the deposition mechanism of the composite coating was proposed.

2. Materials and Methods

2.1. Elaboration of Pd-Ni/TiO_2 Composite Coatings

All the composite coatings were electrodeposited on 316L stainless steel (316L SS) sheets (40 mm × 13 mm × 2 mm). The composition of 316L SS (wt.%) is as follows: Cr 17.14%, Ni 12.58%, C 0.014%, Mo 2.28%, Si 0.6%, Mn 0.8%, P 0.013%, S 0.0073%, and Fe balanced. First, SS substrates were ground with SiC abrasive paper up to 1000 grit and then degreased in an alkali solution at 70 °C for 10 min to remove oil and grease. The alkali solution consisted of 50 g L^{-1} NaOH, 40 g L^{-1} Na_3PO_4, 40 g L^{-1} Na_2CO_3, and 5 mL L^{-1} $C_8H_{17}C_6H_4O(CH_2CH_2O)_{10}H$ (Emulsifier OP-10). Next, a cathodic current of 10 A dm^{-2} was applied on SS substrate for acidic activation in a 20 wt.% H_2SO_4 + 80 g L^{-1} $(NH_4)_2SO_4$ solution (the pH was approximately 1) for 5 min, and the substrate was rinsed with deionized water. When the pretreatment was finished, the composite coating was electrodeposited on an activated SS substrate. The electrolyte composition and deposition conditions are presented in Table 1.

Two bulk samples of graphite (each with dimensions of 10 mm × 15 mm × 0.5 mm) were linked with a copper wire and worked as double anodes. The distance between the two anodes was approximately 6 cm. Figure 1 depicts the schematic of electrodeposition setup. Hydrophilic

anatase TiO_2 powders with an average size of 25 nm were used in the electrodeposition experiment. Particularly, the electrolyte for deposition was ultrasonically dispersed for 20 min before deposition to prevent the TiO_2 particles agglomeration in the solution. The electrolytic bath was mechanically stirred with a magnetic stirrer at 300 rpm during electrodeposition. The deposited specimens were labeled from 0 g L^{-1} to 15 g L^{-1}, which represented the specimens that were deposited from the electrolyte that contained various TiO_2 contents in the paper.

Table 1. The composition of the electrodeposition bath and pulsed current processing parameters.

Chemicals	Amount (g L^{-1})	Processing Prameters
$PdCl_2$	3.6	Current density = 1 A dm^{-2}
$NiSO_4 \cdot 6H_2O$	21	pH = 8–8.5
NH_4Cl	60	Temperature = 40 °C
$Na_3C_6H_5O_7$ (trisodium citrate)	21	Frequency = 1 Hz
TiO_2	0, 5, 10, 15	Duty cycle = 0.8
$NH_3 \cdot H_2O$ (28%)	40 mL L^{-1}	Deposition time = 300 s
$N(CH_2CH_2OH)_3$ (TEOA)	1 mL L^{-1}	–

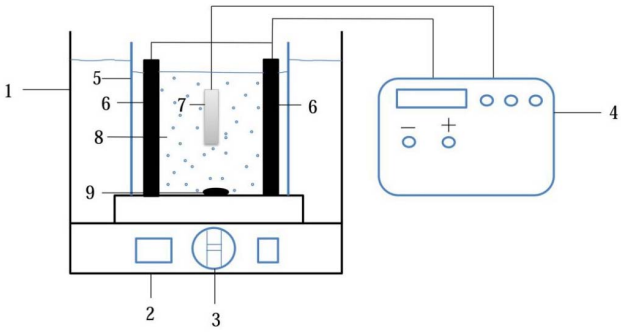

Figure 1. Schematic illustration of the electrodeposition setup: 1-Water bath, 2-Temperature controller, 3-RPM, 4-Power supply, 5-Container, 6-Anode, 7-Cathode, 8-Electrolyte containing TiO_2 particles, 9-Magnetic stirrer.

2.2. Characterization of Pd–Ni/TiO_2 Composite Coatings

The crystallographic coatings structures were measured with X-ray diffraction (XRD, X'Pert PRO, PANalytical, Almelo, Netherlands, Cu-Kα, V = 40 kV, I = 20 mA, λ = 1.548 Å). The surface morphologies and cross sections of the specimens were analyzed by scanning electron microscopy (SEM, EVO MA15, Zeiss, Oberkochen, Germany). The chemical compositions of the composite coatings were analyzed with energy dispersive spectrometry (EDS, X-MaxN, Oxford Instruments, Oxford, UK). Glow discharge optical emission spectroscopy (GDOES, GDA 750HR, Spectruma Analytik Gmbh, Hof, Germany) was conducted for the analysis of the composite coatings using argon as the working plasma gas.

2.3. Microhardness Measurements

The microhardness measurements were performed using a microhardness tester (Fischer HM2000, Windsor, CA, USA) with a load of 20 mN and a dwell time of 20 s. The corresponding 20 final values were presented, and the average values of the 20 measurements in random locations were also provided.

2.4. Weight Loss Experiments

Weight loss tests were conducted to evaluate the corrosion rates of the various coated samples in aerated 20 wt.% H_2SO_4 solutions at 60 °C for 72 h. This solution was been chosen to simulate

the aggressiveness of media in fuel cell. These specimens were obtained from an electrolytic bath containing different concentrations of TiO_2 particles. Moreover, bare 316L SS was employed for comparison. The size of all the specimens used in this experiment was 40 mm × 13 mm × 2 mm. Three equivalent specimens obtained under the same conditions were used to calculate the average corrosion rates. Prior to the weight loss tests, the specimens were weighed on a balance that was accurate to 10^{-5} g. After the experiments, the samples were cleaned with deionized water, dried in a vacuum dryer, and weighed again. Finally, the average corresponding mass loss per unit of surface area of the coatings was calculated.

2.5. Electrochemical Corrosion Behavior

A conventional three-electrode cell was employed to evaluate the electrochemical behavior of the composite coatings with an electrochemical workstation (CHI660E, CH Instrument, Inc., Wuhan, China). The coated samples and bare 316L SS were connected with rubber-covered copper wires as the working electrodes and sealed with silica gel. Approximately 1 cm^2 areas were exposed as working surface. All sealed samples were stored in the drying basin for three days before the electrochemical tests. A mercurous sulfate electrode (MSE, E = 613 mV vs. SHE) was the reference electrode, whereas a platinum foil (0.6 cm^2) was the counter electrode. The solution for the electrochemical experiment was aerated 20 wt.% H_2SO_4 solution maintained at 60 °C.

Open circuit potential (OCP) monitoring was conducted for 30 min, followed by electrochemical impedance spectroscopy (EIS) measurements. EIS testing was performed at the frequency range of 100 kHz–10 MHz with an amplitude of 10 mV at the OCP. The impedance plot fittings were performed by ZSimpWin software V 3.20.

Potentiodynamic polarization curve tests were carried out over the range from 100 mV below the OCP to 800 mV above the OCP at a scanning rate of 0.5 mV s^{-1}. The criteria of reactivity of the sample were chosen as the corrosion current that was extrapolated at the corrosion potential from cathodic Tafel extrapolation. The authors do not consider this exchange current as a rigorous corrosion current density, but it is sufficiently indicative to propose a ranking of the samples in this work.

3. Results and Discussion

3.1. Characterization of the Composite Coatings

The XRD patterns of TiO_2, the 316L SS substrate, and the Pd-Ni and Pd-Ni/TiO_2 composite coatings are shown in Figure 2. Note that the crystalline structure of TiO_2 displays a refined anatase TiO_2 structure. The Pd peaks are displayed at 40.1°, 46.7°, 68.1°, and 86.6°, whereas the Ni peaks are located at 44.5°, 51.8°, 76.4°, and 92.9° [23], because metallic palladium and nickel are both face-centered cubic (FCC) crystalline phases according to Bragg's equation. The peaks at approximately 2θ = 42.2°, 49.2°, 70.4° and 86.9° correspond to the (111), (200), (220) and (311) planes of Pd-Ni alloy, respectively (JCPDS card No: 65-5788), and each peak is between the corresponding peaks of Pd and Ni. It is indicated that all tested coatings exhibit an FCC crystalline phase according to $\sin^2\theta_1:\sin^2\theta_2:\sin^2\theta_3:\sin^2\theta_4 = [(h_1)^2 + (k_1)^2 + (l_1)^2]:[(h_2)^2 + (k_2)^2 + (l_2)^2]:\ldots:[(h_4)^2 + (k_4)^2 + (l_4)^2] = 3:4:8:11$ (Bragg's equation and the systematic absence law of the crystal's X-ray diffraction) and a substitution solid solution is formed [8]. Furthermore, the (200) plane is predominant, and the diffraction peak of the (200) plane is broadened and gradually shifts to a higher angle with an increase in TiO_2 particle concentrations in the electrolyte. The reason for the change of lattice will be discussed afterward. The (200) plane crystal grain size of the composite coatings that contain various concentrations of TiO_2 is calculated according to Scherrer's equation as follows [24].

$$D = 0.9\lambda/(\beta \times \cos\theta) \quad (1)$$

where D is the crystal grain size, λ is the wave length of the incident radiation, β is the corrected peak width at half-maximum intensity, and θ is the angular position. The calculated results show

that the crystal grain size in the composite coatings gradually decreases from 22 nm to 21 nm, 17 nm, and 14 nm with increasing TiO_2 content in the electrolyte. The TiO_2 particles were suspended in the electrolyte and adsorbed on the metal matrix during deposition that could increase crystal nucleation and retard crystal growth [13,25]. Note that the TiO_2 peaks could not be detected. This finding could be due to the higher intensities of the diffraction peaks of the Pd-Ni alloy compared with those of TiO_2, and the low contents of TiO_2 in the film [26].

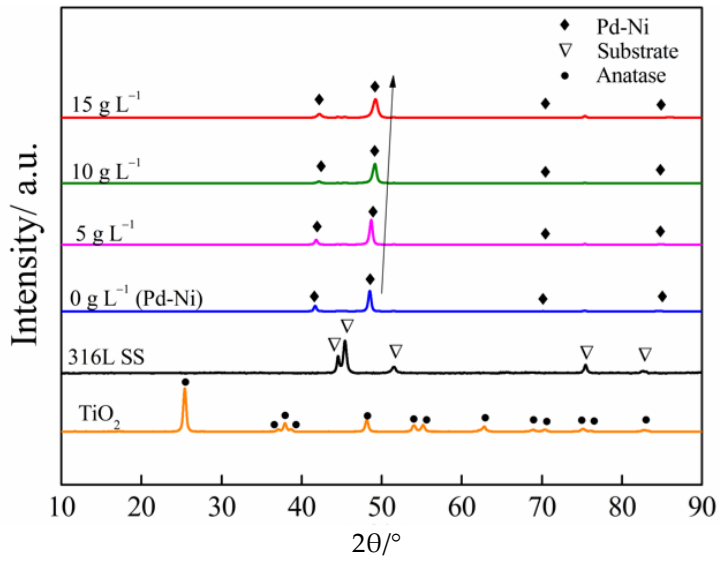

Figure 2. The X-ray diffraction (XRD) patterns of TiO_2, 316L SS, Pd-Ni coating, and Pd-Ni/TiO_2 composite coatings with different concentrations of TiO_2 in electrolyte.

Figure 3 shows SEM micrographs of coatings that were obtained from the electrolytic bath with various TiO_2 concentrations. The chemical compositions of the composite coatings were analyzed by EDS, and the results are depicted in Figure 3. The Pd-Ni alloy film shows a compact surface microstructure (Figure 3a). Because of the addition of TiO_2 particles into the electrolyte, note that the surface morphologies of the deposited samples exhibit obvious differences. For example, when 5 g L^{-1} TiO_2 particles were introduced into the electrolytic bath, spherical particles could be observed on the surface of the deposited coating (Figure 3b). The coating prepared from the electrolyte with 10 g L^{-1} TiO_2 displays a greater quantity of spherical particles on its surface. It is remarkable that the surface of the coating that was obtained from the bath containing 15 g L^{-1} TiO_2 shows specific areas with a high content of titanium, as shown in Figure 3d. Since TiO_2 nanoparticles can provide more crystal nucleation sites for crystal growth, TiO_2 particles might play a key role in modifying of the morphology and structure of the coatings [27]. The content of titanium dioxide in the composite coatings increases with an increase in TiO_2 particle content in the electrolyte. When excessive TiO_2 particles (15 g L^{-1}) were employed in electrolytic solution, nanosized TiO_2 particles promote an aggregation tendency in the electrolytic solution due to their small size and high surface energy [21,28]. As a result, the partial distribution of titanium in composite coating can be characterized.

To further understand the distribution of titania in a composite coating and elemental mapping of a special area on the specimen that was obtained from the electrolyte containing 15 g L^{-1} TiO_2 are presented in Figure 4. In the mappings, Pd and Ni are uniformly distributed, whereas Ti and O display opposite results. EDS spectra of this sample were obtained at different locations. The elemental compositions (wt.%) in a Ti-rich area (point B in Figure 4a) are 69.70% Pd, 18.28% Ni, 5.87% Ti, and 6.15% O, whereas the contents in another area (point A in Figure 4a) are 77.73% Pd, 21.76% Ni, 0.18% Ti, and 0.33% O. There are remarkably different contents of Ti in the two areas. Therefore, the

results confirm that the excessive addition of TiO_2 particles promote its agglomeration and create a non-uniform morphology in the composite coating.

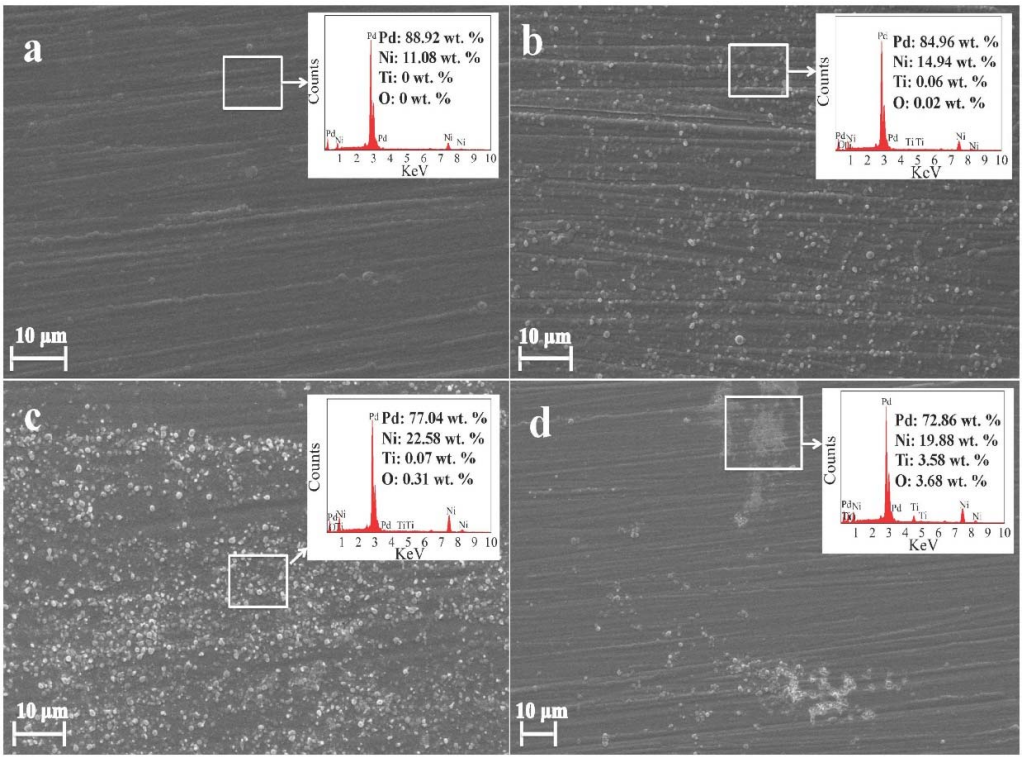

Figure 3. Scanning electron microscopy (SEM) images of coatings obtained from electrolyte containing (**a**) 0 g L^{-1} TiO_2; (**b**) 5 g L^{-1} TiO_2; (**c**) 10 g L^{-1} TiO_2; and (**d**) 15 g L^{-1} TiO_2.

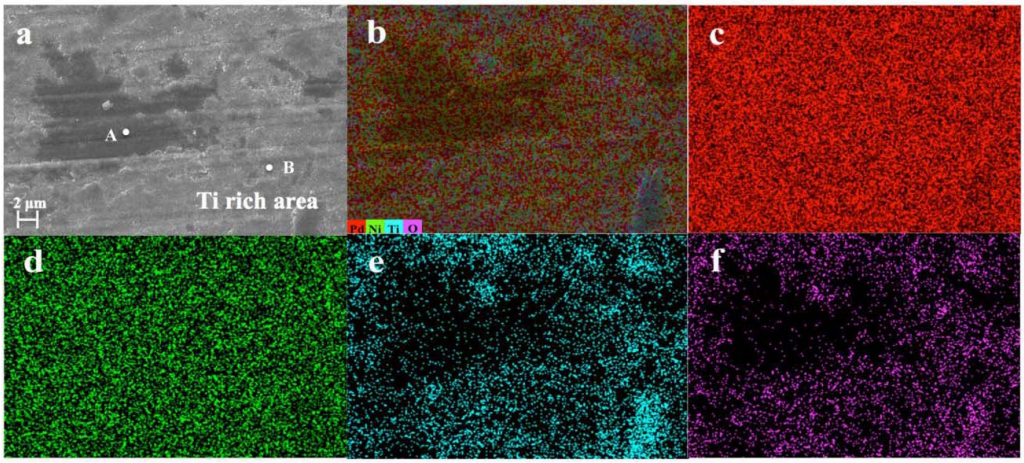

Figure 4. Elemental mapping analysis by energy dispersive spectrometry (EDS) for the composite coating obtained from 15 g L^{-1} TiO_2 containing electrolyte. (**a**) SEM image of selected area; (**b**) Mapping of all elements; (**c**) Pd mapping; (**d**) Ni mapping; (**e**) Ti mapping; and (**f**) O mapping.

Previous characterizations considered only the coating surface to understand the distribution of nanoparticles in the coating matrix. Hereafter, the cross section of the Pd-Ni/TiO_2 composite coating is considered. First, a cross-sectional SEM image of the Pd-Ni/TiO_2 composite coating that was obtained from the electrolyte containing 15 g L^{-1} TiO_2 is shown in Figure 5. Some microdefects may exist somewhere in the coating according to the mechanism of electrodeposition (i.e., the cathodic hydrogen

evolution reaction). However, the composite coating is smooth and compact with good adhesion on the 316L SS substrate. There are no cracks or gaps. The GDOES was adopted to obtain further information regarding the TiO_2 content and distribution in the coating. Figure 6 presents GDOES depth profiles for chemical element analysis in the composite coatings with various concentrations of TiO_2 particles, and the main elements in 316L SS (Fe and Cr) are presented. Furthermore, the other alloying elements in 316L SS, such as Mn, Mo, and Si, were removed to simplify the profiles.

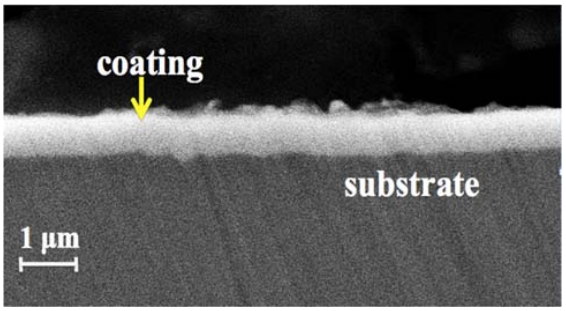

Figure 5. Cross-sectional SEM image of the coating obtained from 15 g L^{-1} TiO_2 in electrolyte.

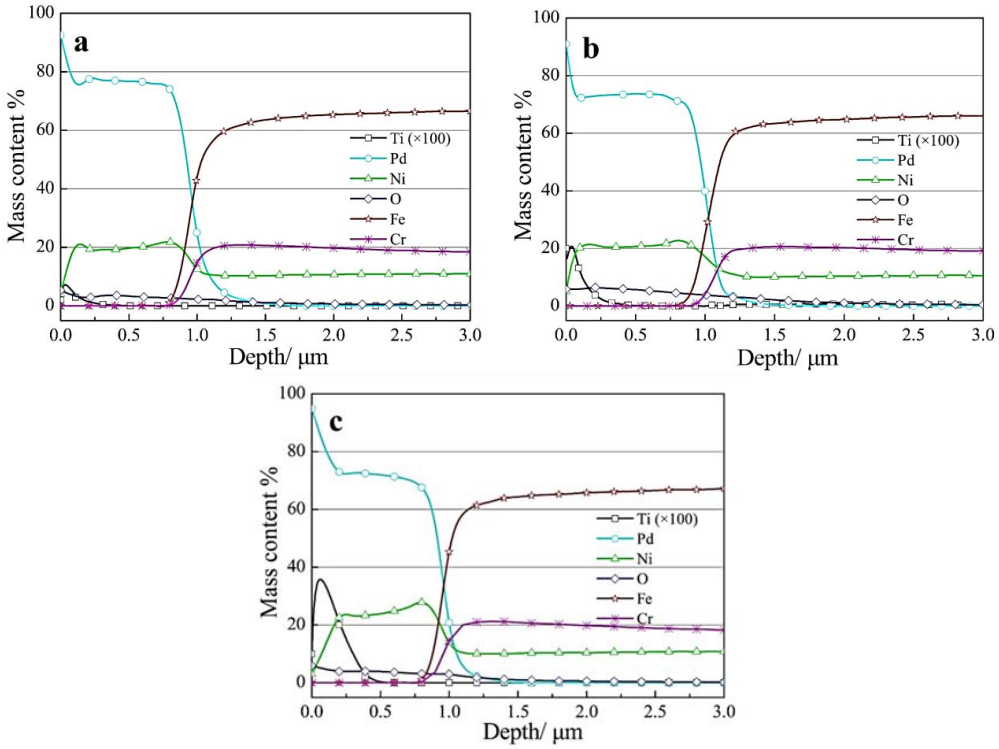

Figure 6. Glow discharge optical emission spectroscopy (GDOES) depth profiles of the coating deposited from (**a**) 5 g L^{-1} TiO_2; (**b**) 10 g L^{-1} TiO_2 and (**c**) 15 g L^{-1} TiO_2 concentration solution.

Clearly, the thickness of the composite coatings is approximately 1 μm, and all curves for the mass contents of Pd and Ni show similar shapes in the three figures. There is no doubt that the content of Ti element in composite coatings exhibit an upward trend with an increase in TiO_2 particles in the electrolyte. According to Guglielmi's two-step adsorption model [29], first, the particles would loosely adsorb on the cathode, which is dominated by the particle concentration in the electrolyte, whereas the second step mainly depends on the overpotential, which is a type of strong adsorption. Hence, when the operating conditions are constant, the number of insoluble particles in the electrolytic solution

determines the inert particles contained in the composite coatings. Note that TiO_2 particles are mostly distributed in the external part (0.5 μm) of the entire coating. Similar research results were also found by Grari et al. [30] and Calderón et al. [31]. First, as explained hereafter, mobility of metallic cations is higher than oxide particles. Thus, cations adsorption will be electrically assisted. Adsorption of oxide particles needs to be surrounded by metallic cation before being adsorbed. The competition between this two-step privilegiate is the metallic part in inner layer and oxide in outer layer. Second, these results could be related to the stronger electronic affinity of the Pd-Ni alloy compared with that of the 316L SS surface to oxide complexes [32]. Therefore, a small quantity of Ti element is found in the interior parts of the coatings near the coating/316L SS interface. In addition, a slightly decrease in Ti element, a decrease in Ni element and an increase in Pd element in the outermost layer of the coating are observed. It is probably because of the power-off-delay effect. The double layer at coating/solution interface can be considered as a plane-parallel capacitor after the power-off of the electrodeposition circuit. Capacitor discharge continues for a while but the double layer potential decreases with the time evolution after the power-off of electrochemical workstation. Owing to the overpotential of Pd electrodeposition is smaller than that of Ni, more Pd will be electro-reduced with the double layer potential decreasing at the last.

With increasing TiO_2 particles in the electrolytic bath, the Pd content in the coatings decreases, whereas that of Ni exhibits a rising trend, as shown in Figure 6, which agrees with the EDS analysis. Since the atomic radius of Pd is 0.1370 nm and that of Ni is 0.1240 nm, the Pd atoms and Ni atoms form the complete solid solution with an FCC structure. When a growing number of Pd atoms are replaced by Ni atoms in the Pd-Ni solid solution, the average lattice constant decreases [8]. As a result, the peaks of the Pd-Ni alloy in the composite coating shift to a higher angle, as shown in the XRD patterns (Figure 2). In addition, there are plateaus in the mass content profiles of Pd and Ni from the coating/substrate interface that is close to the surface (approximately 0.2 μm), which means a constant composition in the interior layer. However, the content of Pd increases, whereas that of Ni decreases with a reduction in the coating depth, and finally the outermost layer of the coating has the highest Pd content up to 90 wt.% or more and the lowest Ni content. Consequently, with the further addition of TiO_2 particles in the electrolytic bath, the contents of Pd and TiO_2 contained in the outer layer of the coating increase, whereas the Ni content in the inner layer of the coating increases. A further understanding of the deposition process can be achieved with the schematic diagram presented in Figure 7.

In Figure 7, Pd and Ni correspond to their cations and metallic complexes and also partly adsorb on hydrophilic TiO_2 particles in the solution. All elements are expected to be uniformly distributed in the electrolytic bath before electrodeposition (Figure 7a). When a voltage was applied to 316L SS, Pd and Ni were reduced on the 316L SS surface first (Figure 7b). Pulse current-assisted complex ions and nanoparticles can move to the surface of the cathode more easily. Furthermore, less adsorbed hydrogen is generated during pulse deposition [22]. The palladium content is always higher than that of nickel in the coating compared with their contents in the electrolytic bath, which indicates that the reduction rate of Pd is faster than that of Ni. Normally, a higher redox potential and deposition current efficiency results in preferential metal electrodeposition.

At the same time, nanosized TiO_2 particles migrate to the cathode under an electric field and electrophoresis in the electrolyte. However, the electronic affinity of TiO_2 particles to 316L SS is weak, therefore, it is difficult for TiO_2 particles to adsorb on the SS substrate. Meanwhile, the TiO_2 particles that were physically adsorbed on the 316L SS were easily removed by mechanical stirring due to the poor binding with 316L SS. As a result, the deep part of composite coating was composed of the Pd-Ni alloy during the first stage of electrodeposition. During this period, the mass contents of Pd and Ni were almost constant. On the other hand, more Pd ions and its complex were adsorbed on titania particles. This adsorption could result in a decrease in the effective concentration in the first stage. Therefore, the general mass content of Ni in the composite coating was obviously higher than that in the Pd-Ni alloy coating (EDS analysis). Additionally, the interior Ni content increased with an increase

in TiO_2 particles in the electrolyte. After the first stage, when the substrate surface is covered by the Pd-Ni alloy inner layer, the electronic affinity to TiO_2 particles is enhanced, and the TiO_2 particles start to stably adsorb on the growing coating matrix (Figure 7c).

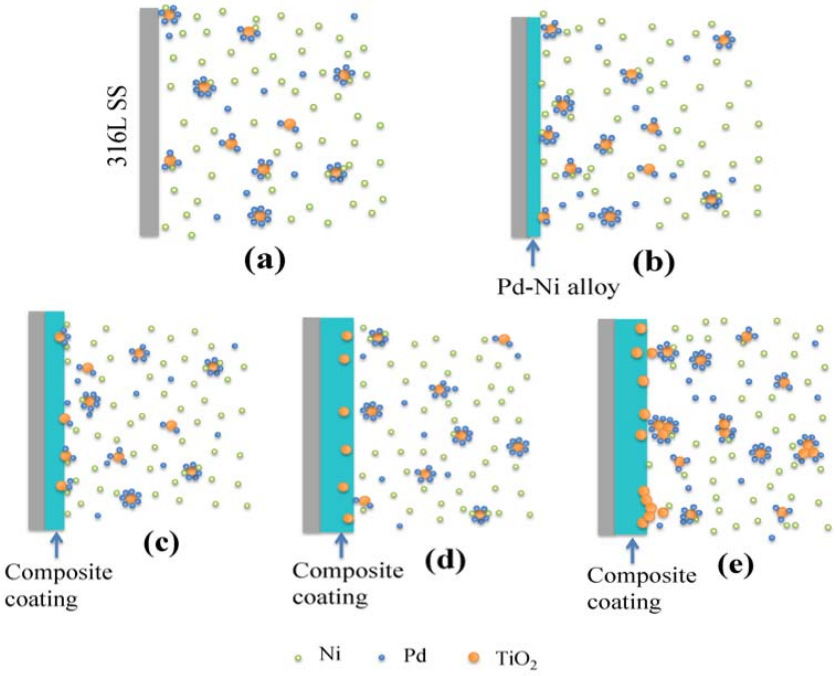

Figure 7. Deposition process schematic diagram of Pd-Ni/TiO_2 (**a**) Before electrodeposition; (**b**) Initial stage of electrodeposition; (**c**) TiO_2 particles incorporated in the growing coating matrix; (**d**) TiO_2 particles embedded in the coating matrix completely and (**e**) aggregated TiO_2 particles embedded in the coating matrix.

In the final stage, TiO_2 particles were totally embedded in the metal matrix with a reduction in ions, and the composite coating was formed (Figure 7d). In this stage, the Pd content increased while the Ni content decreased in the composite coating, and accordingly, more palladium ions and their complexes were carried with the TiO_2 particles and reduced. If excessive titania particles were introduced in the electrolytic bath, some would be aggregated. Those aggregated particles would be buried in the coating resulted in the partial distribution of titanium in composite coating (Figure 7e) following the same deposition mechanism as described before. From the former observations, all the XRD, SEM and EDS results showed good agreement and strongly support the electrodeposition model.

3.2. Microhardness Measurements

All tested microhardness values of the Pd-Ni alloy coating and Pd-Ni/TiO_2 composite coatings and the average microhardness values of these samples are shown in Figure 8. Apparently, the composite coatings have a wider range of microhardness values in comparison with that of the Pd-Ni alloy coating. Additionally, the microhardness values of the Pd-Ni/TiO_2 composite coatings increase with an increase in TiO_2 particles in the electrolytic bath. The average microhardness value of the Pd-Ni alloy is approximately 481.7 HV. With the addition of 5 g L^{-1} TiO_2 in electrolytic bath, the average microhardness value of obtained specimen increases to 500.1 HV, and the average microhardness values of other specimens that were deposited from the electrolyte containing 10 g L^{-1} and 15 g L^{-1} TiO_2 are 500.9 HV and 507.6 HV, respectively. Dispersion in the measurement can be explained by combination between the roughness of the coatings and the weak applied load.

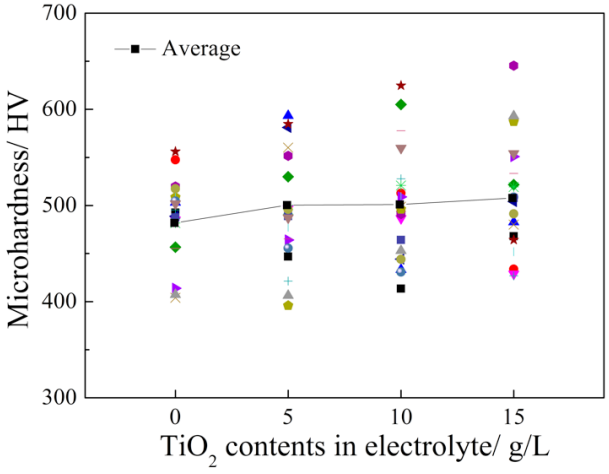

Figure 8. Microhardness values of various samples.

The existence of nanosized TiO_2 particles improved the coating hardness by forming a second phase with superior mechanical properties. Furthermore, a decrease in the alloy grain size in the coating could be another reason for the increased microhardness [22]. According to the calculated crystal grain size of the Pd-Ni phase and the hardness test, the specimen with smallest crystal grain size and the highest Ti content displays the highest microhardness value, indicating that the enhanced microhardness of Pd-Ni/TiO_2 composite coatings are due to the strengthening resulting of the particles dispersion and the grain refining [33].

3.3. Weight Loss Tests

After 72 h of immersion in an aerated 20 wt.% H_2SO_4 solution at 60 °C, the corrosion rates of the composite coatings were calculated using their mass variations before and after weight measurements. For 316L SS, the corrosion rate reached 141.78 g m^{-2} h^{-1} after immersion for 2 h and 41.91 g m^{-2} h^{-1} after 72 h. In the corrosion condition of 20% sulphuric acid solution at 60 °C, drastic active dissolution occurs that the corrosion rate of bare 316L SS decreases with time evolution because the consumption of H^+ is very fast. However, the corrosion rates of the coated specimens significantly decreased after deposition. The corrosion rate of the Pd-Ni deposited SS was 0.0023 g m^{-2} h^{-1} for the same immersion duration. For the addition of 5 g L^{-1}, 10 g L^{-1}, and 15 g L^{-1} TiO_2 particles into the electrolyte, the corrosion rates of the deposited specimens were 0.0012 g m^{-2} h^{-1}, 0.0015 g m^{-2} h^{-1}, and 0.0019 g m^{-2} h^{-1}, respectively. It is evident that the coatings inhibited the corrosion of 316L SS in hot sulfuric acid solution and the corrosion resistance of the coatings are almost 10^5 times than that of bare 316L SS. Moreover, the corrosion rates of Pd-Ni/TiO_2 composite coatings exhibit lower corrosion rates than that of the Pd-Ni alloy coating, which indicates that the small amount of titania particles in the coating can benefit the corrosion resistance. In addition, the composite coating that was deposited from the electrolyte containing 5 g L^{-1} has the lowest corrosion rate, and with 15 g L^{-1} TiO_2 particles in electrolytic bath, the corrosion rate of the obtained specimen increased. That could be explained by the fact that low TiO_2 content exhibits dispersed particles and more homogeneous coating. High TiO_2 content induces agglomeration. These agglomerated particles induced connected pathway for aggressive media which induces under deposit corrosion. This corrosion mode can be associated to crevice corrosion which exhibit autocatalytic phenomena and aggressiveness increasing of the media. Anyway, whatever the TiO_2 content, corrosion rate is lower that Ni-Pd coating or bare stainless steel.

3.4. Electrochemical Tests

The OCP curves of various samples versus time in 60 °C sulfuric acid solution are depicted in Figure 9. For the 316L SS sample, the active dissolution with hydrogen evolution is observed during OCP measurements. Clearly, the OCP of the coated specimens have significantly increased compared with that of the stainless steel sample. A higher OCP indicates that the as-prepared coatings are a cathodic coating with regards to the 316L SS substrate. The potentials of all the coated specimens are stable during the test duration, and no corrosion phenomenon is observed during the measurements. In addition, the sample with the Pd-Ni alloy coating has a lower OCP than those of the samples with the Pd-Ni/TiO_2 composite coating. Therefore, the addition of titania can increase the OCP of the Pd-Ni alloy, even with a reduction in the Pd content in the film (Figure 3). However, the OCP values of the sample with the composite coating are similar after 900 s, which suggests that there is no significant influence of the oxide particles adding on the thermodynamic property.

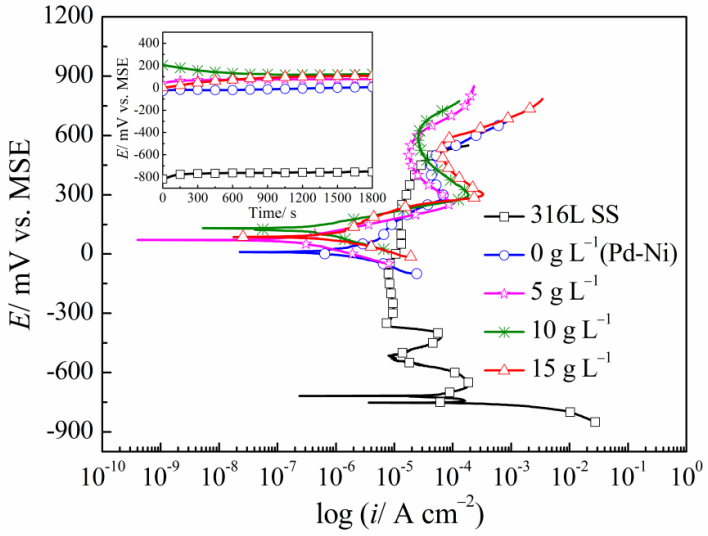

Figure 9. Open circuit potential (OCP) monitoring and potentiodynamic polarisation curves with scanning rate of 0.5 mV s^{-1} of 316L SS and as-deposited coatings from electrolytes with different TiO_2 concentrations in 20 wt.% H_2SO_4 solutions at 60 °C.

The polarization curves that were measured on the 316L SS and Pd-Ni alloy film samples and the Pd-Ni/TiO_2 composite coatings electrodeposited using different TiO_2 concentrations in the electrolyte are shown in Figure 9. The polarization curve of 316L SS shows the active-passive oscillating behavior of stainless steel in sulfuric acid [34]. First, the corresponding corrosion current density at corrosion potentials of −750 mV vs. MSE is high, active dissolution occurs, and the stable passivation of the specimen can only be achieved above −300 mV vs. MSE. The 316L SS sample can only passivate by raising the potential to the anodic range of −300 to 400 mV vs. MSE. In comparison, the corrosion potentials of the coated samples significantly increase and turn positive in the anodic passivation domain. Thus, the stable passivation of the substrate is achieved by the anodic polarization effect of coatings [1,6], which is in agreement with information from the OCP measurements. In addition, the deposited coatings can provide a protective barrier layer for the 316L SS substrate owing to the good corrosion resistance of coating itself. Consequently, because of the anodic polarization and barrier effects of Pd-Ni or Pd-Ni/TiO_2 composite coatings, coated 316L SS is protected and shows corrosion resistance in hot dilute H_2SO_4 solutions. Furthermore, according to the electrochemical polarization mechanism in the passivable 316L substrate, even deposited Pd-Ni/TiO_2 composite coatings may contain pin holes or defects, the localized exposed areas of the 316L SS substrate still can maintain

passivation in the stable state. An outstanding advantage of this coating is to protect stainless steel in hot dilute sulfuric acid in two aspects.

However, all polarization curves of the coated samples display a current step at a potential of approximately 300 mV vs. MSE. It might be related to the oxidation of palladium in composite coatings (Pd/Pd^{2+} equilibrium potential +302 mV vs. MSE). The potential and current density of the current step slightly increase with a decrease in Pd content in the composite coating. The corrosion potentials (E_{corr}) and corrosion current densities (i_{corr}) of all specimens were obtained using the Tafel extrapolation method. They are shown in Table 2 together with OCP and cathodic Tafel slopes. Because there is a current oscillation at −710 mV vs. MSE in the anodic polarization curve near the corrosion potential of 316L SS, and the potential at −750 mV vs. MSE is considered as the corrosion potential. The results of cathodic Tafel fitting are in good agreements with those of OCP measurements and mass loss measurements.

Table 2. OCP, corrosion potentials, current densities, and cathodic Tafel slopes of 316L SS and the composite coatings deposited from electrolytes with various TiO_2 concentrations.

Samples	OCP (mV vs. MSE)	E_{corr} (mV vs. MSE)	i_{corr} ($\times 10^{-7}$ A cm^{-2})	β_c (mV dec^{-1})
316L SS	−721	−750	882.70	49
Pd-Ni	5	10	13.80	101.19
Pd-Ni/TiO_2 (5 g L^{-1})	78	71	2.14	76.48
Pd-Ni/TiO_2 (10 g L^{-1})	122	140	2.47	77.82
Pd-Ni/TiO_2 (15 g L^{-1})	106	101	7.02	70.87

The electrochemical impedance of the Nyquist plots of samples with and without coatings in sulfuric acid at a high temperature is presented in Figure 10a. The Nyquist plots of 316L SS show the lowest impedance and have three parts. These data can be attributed to the high corrosion rate and probably the existence of intermediate corrosion products because the bare 316L SS was in an active dissolution state or active-passive transition state in hot 20 wt.% H_2SO_4 solution during the EIS measurement. Note that the coated specimens show significantly higher impedance values in comparison with that of the blank sample. Compared with the specimen-coated Pd-Ni alloy, the coating obtained from the electrolyte containing 5 g L^{-1} TiO_2 has a larger impedance loop. However, with the further addition of TiO_2 particles into the electrolytic bath, the impedance values of the obtained samples decrease.

Bode plots of various specimens in sulfuric acid solution are displayed in Figure 10b. Two time constants are found in all coated samples, except for uncoated 316L SS. For bare 316L SS, the additional time constant corresponds to the feature of its Nyquist plot. For the coated samples, the time constant at the higher frequency is related to the charge transfer process through the interface, whereas the low-frequency region is concerned with simultaneous physicochemical phenomena at the solution/electrode interface [35]. The equivalent circuit model exhibited in Figure 10c is employed to explain the corrosion behavior of the coated samples [6]. In this case, R_s is the solution resistance; Q_{dl} and R_{ct} represents the double-layer capacitance and the charge transfer resistance, respectively; whereas Q_c and R_c correspond to the capacitance and resistance of the electrochemical reaction at the interface, respectively. In an equivalent electrical circuit, Q constant phase elements (CPE) are considered to obtain more accurate fitting results.

$$Z_{CPE} = Q^{-1}(j\omega)^{-n} \quad (2)$$

where Z_{CPE} is the impedance of the constant phase elements, Q is the admittance magnitude of CPE, ω is the angular frequency of alternating current voltage, and n is the exponential term. Pure capacitance behavior is represented by n = 1, whereas in practice n often ranges from 0 to 1. A perfect resistance is represented by n = 0. The fitted parameters are shown in Table 3.

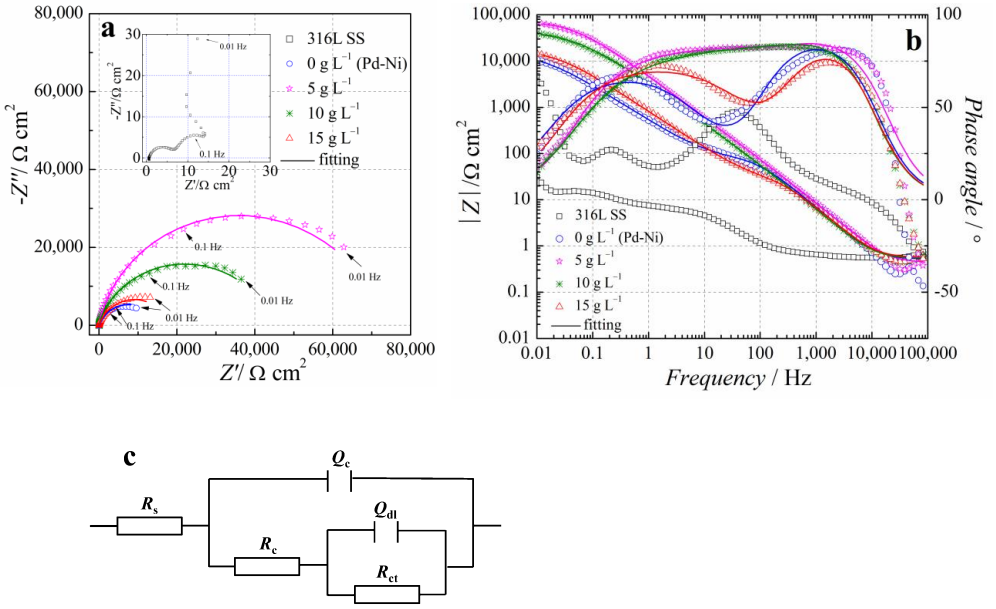

Figure 10. Electrochemical impedance (**a**) Nyquist plots, (**b**) Bode diagram and (**c**) Equivalent electrical circuit model for fitting EIS of coatings from electrolytes with different TiO_2 concentrations in 20 wt.% H_2SO_4 solution at 60 °C.

Table 3. Equivalent circuit parameters of the electrochemical impedance spectroscopy (EIS) results.

TiO_2 Content in Electrolyte (g L^{-1})	0	5	10	15
R_s (Ω cm^2)	0.526	0.55	0.61	0.573
Q_{dl} (S_n Ω^{-1} cm^{-2})	3.171×10^{-5}	2.46×10^{-5}	2.523×10^{-5}	3.07×10^{-5}
n_{dl}	0.965	0.968	0.95	0.942
R_{ct} (Ω cm^2)	90.48	134.1	111	97.39
Q_c (S_n Ω^{-1} cm^{-2})	4.307×10^{-4}	1.95×10^{-5}	4.676×10^{-5}	2.348×10^{-4}
n_c	0.786	0.671	0.684	0.793
R_c (Ω cm^2)	1.442×10^4	7.68×10^4	4.825×10^4	1.763×10^4
χ^2 (10^{-2})	7.73	4.65	8.42	2.63

Table 3 provides the electrochemical parameters from the fitting using the model in Figure 10c for coatings deposited from various amounts of TiO_2 particles in the electrolytes. The sample prepared from the electrolyte containing 5 g L^{-1} TiO_2 has the largest resistance of anodic dissolution reaction (R_c) value among all samples and is approximately 5 times of that of the Pd-Ni coating without TiO_2. Additionally, the charge transfer resistance (R_{ct}) of this sample also has the maximum value. These results demonstrate that the composite coating deposited from the electrolytic solution containing 5 g L^{-1} TiO_2 has the best corrosion resistance in this corrosive medium. This might be attributed to the role of TiO_2 particles in modifying the structure of the coating. TiO_2 particles have been found to have high chemical stability and corrosion resistance [36]. The nanosized TiO_2 particles were adsorbed and incorporated into the Pd-Ni coating matrix and inhibited the initiation and propagation of cracks, gaps, or microholes during the deposition, which could result in a more compact microstructure of the composite coating [37]. Particularly, these TiO_2 nanoparticles act as inert physical barriers to the initiation and development of a corrosion defect and can thus substantially improve the corrosion resistance of the composite coating [36].

When excessive TiO_2 particles are introduced into the electrolytic bath, the protection effect of composite coatings decreases due to the agglomeration of TiO_2 nanoparticles. The agglomeration is driven by a combination of van der Waals forces, mechanical movement and gravity under continuous agitation in an electrolytic bath [21]. As a result, a localized non-uniform or inhomogeneous morphology is formed (Figure 3d). Apparently, with an increase in TiO_2 in the electrolyte, R_c decreases

because of increasing defects in the coatings (Table 3). This result indicates that the physical barrier effect of the coating is weakened and more of the 316L SS substrate surface is exposed to corrosive solution, which increases the difficulty of passivation and anodic dissolution.

Alternatively, since Pd, as a noble metal, plays a significant role in promoting the passivation of 316L SS by its strong anodic polarization effect [38], the increasing Ni content in the coating has negatively influences the formation of a passive film at the 316L SS/H_2SO_4 solution interface. From the two reasons above, both the R_{ct} and the R_c of the composite-coated sample decreases with an increase in the TiO_2 content, as shown in Table 3. The total resistance value (R_c + R_{ct}) of the sample that was deposited from the 15 g L^{-1} TiO_2 electrolyte is only 40% and 25% the value of the samples from the 10 g L^{-1} and 5 g L^{-1} TiO_2 electrolytes, respectively. Correspondingly, the corrosion rate of that sample increased 27% and 58% in the weight loss test. This finding reveals that the distribution of TiO_2 particles is important for the properties of the composite coating. Although a further introduction of nanosized titania particles in the electrolyte caused the Pd content to decrease in the coating and weakened its electrochemical polarization effect compared with the anti-corrosion properties of the Pd-Ni alloy coating, the Pd-Ni/TiO_2 composite coatings still exhibited better corrosion resistance. Q_c and Q_{dl} of all the Pd-Ni/TiO_2 composite-coated samples are smaller than those of the Pd-Ni-coated sample. This finding reveals that the composite coating has slower corrosion kinetics, which is in good agreement with the demonstration of R_c and R_{ct}. Because the inhomogeneity of the Pd-Ni/TiO_2 composite coating increases with an increase in TiO_2 content, the n_{dl} value decreases in composite coated samples. However, all values of n_c are obviously smaller than 1, which might be associated with the diffusion-migration process at the electrode/sulfuric acid solution interface [39].

The remarkable improvement in mechanical and corrosion performance at the same time by adding titania particles has not yet been achieved in this study. At present, the agglomeration of nanosized titania particles limit the content of these particles in the composite coating. Thus, more favorable surfactants are needed in this system to disperse the titania particles, which should be performed in future work. Meanwhile, other methods could be used to prepare more uniform composite coatings, such as ultrasonic-assisted electrodeposition. In future work, the contact resistance, tribology characteristics and erosion-corrosion resistance could also be studied, which need a better dispersion of the nanosized TiO_2 particles in composite coatings.

4. Conclusions

In summary, Pd-Ni/TiO_2 composite coatings with approximately 1 μm thickness were obtained from an electrolytic bath that had various concentrations of TiO_2 using an electrodeposition technique.

(1) With the addition of nanosized TiO_2 particles in the electrolytic bath, the morphology of obtained Pd-Ni/TiO_2 composite coatings was modified. In addition, up to 0.38 wt.% TiO_2 particles were embedded in the alloy matrix from the deposition electrolyte containing 15 g/L TiO_2 based on GDOES depth profiles. Furthermore, the addition of TiO_2 particles can benefit the reduction of Ni in the coating. Most of the interior of the composite coating was composed of the Pd-Ni alloy. The deposition model of the Pd-Ni/TiO_2 composite coatings were proposed based on different characterizations. After the initial electrodeposition of Pd-Ni alloy deposits, TiO_2 started to strong adsorb on and embed into the growing coating matrix. Hence, TiO_2 particles existed only in the exterior layer of the composite coatings, which also had a higher Pd content probably because more Pd ions and its complex were adsorbed on TiO_2 particles in the electrolyte.

(2) The microhardness of the Pd-Ni/TiO_2 composite coatings was improved by increasing the TiO_2 content in the coatings. According to the weight loss and electrochemical test results, the specimen that was prepared from the electrolyte containing 5 g L^{-1} TiO_2 showed the best corrosion resistance in 20 wt.% H_2SO_4 solution at 60 °C. Additionally, the composite coating exhibited a better corrosion resistance compared with that of the Pd-Ni alloy film that was obtained under the same conditions. In contrast, the further introduction of TiO_2 particles into the electrolyte decreased the corrosion resistance of the obtained composite coatings because of agglomeration.

Author Contributions: J.T., Z.Z., and B.N. conceived and designed the experiments; Z.Z. and Y.W. performed the experiments; Z.Z., J.T., Y.W., H.W., and B.N. analyzed the data; J.T., Y.W., H.W., and Y.Z. contributed reagents/materials/analysis tools; Z.Z., J.T., Y.W., and B.N. wrote the paper.

Funding: This investigation is financially supported by Project Grants to Scientific Research Innovation Team of Universities Affiliated to Sicuan Province (Grant No. 18TD0012), the Applied Basic Research Programs of Science and Technology Department of Sichuan Province (Grant No. 2017JY0044), and the Qihang Science Research founding of Southwest Petroleum University (Grant No. 2015QHZ013).

Acknowledgments: The authors thank Tang Tao of Chengdu Kuntai Technology Ltd. Co and SPECTRUMA ANALYTIK GMBH for their help in GDOES characterizations.

Conflicts of Interest: The authors declare no conflict of interest.

References

1. Tang, J.; Zuo, Y. Study on corrosion resistance of palladium films on 316L stainless steel by electroplating and electroless plating. *Corros. Sci.* **2008**, *50*, 2873–2878. [CrossRef]
2. Lavigne, O.; Alemany-Dumont, C.; Normand, B.; Berthon-Fabry, S.; Metkemeijer, R. Thin chromium nitride PVD coatings on stainless steel for conductive component as bipolar plates of PEM fuel cells: Ex-situ and in-situ performances evaluation. *Int. J. Hydrog. Energy* **2012**, *37*, 10789–10797. [CrossRef]
3. Dhandapani, V.S.; Subbiah, R.; Thangavel, E.; Arumugam, M.; Park, K.; Gasem, Z.M.; Veeraragavan, V.; Kim, D.E. Tribological properties, corrosion resistance and biocompatibility of magnetron sputtered titanium-amorphous carbon coatings. *Appl. Surf. Sci.* **2016**, *371*, 262–274. [CrossRef]
4. Zuo, Y.; Tang, J.; Fan, C.; Tang, Y.; Xiong, J. An electroless plating film of palladium on 304 stainless steel and its excellent corrosion resistance. *Thin Solid Films* **2008**, *516*, 7565–7570. [CrossRef]
5. Tang, J.; Zuo, Y.; Tang, Y.; Xiong, J. Composition and corrosion resistance of palladium film on 316L stainless steel by brush plating. *Trans. Nonferrous Met. Soc. China* **2012**, *22*, 97–103. [CrossRef]
6. Li, S.; Zuo, Y.; Ju, P. Erosion-corrosion resistance of electroplated Co-Pd film on 316L stainless steel in a hot sulfuric acid slurry environment. *Appl. Surf. Sci.* **2015**, *331*, 200–209. [CrossRef]
7. Xu, L.; Zuo, Y.; Tang, J.; Tang, Y.; Ju, P. Chromium—Palladium films on 316L stainless steel by pulse electrodeposition and their corrosion resistance in hot sulfuric acid solutions. *Corros. Sci.* **2011**, *53*, 3788–3795. [CrossRef]
8. Ju, P.; Zuo, Y.; Tang, J.; Tang, Y.; Han, Z. The characteristics of a Pd-Ni/Pd-Cu double coating on 316L stainless steel and the corrosion resistance in stirred boiling acetic and formic acids mixture. *Mater. Chem. Phys.* **2014**, *144*, 263–271. [CrossRef]
9. Zhang, Z.; Tang, J.; Wang, Y.; Apreutesei, M.; Wang, H. Electrodeposition of A Novel Pd-Ni-W Ternary Alloy Film on SS316L. *Int. J. Electrochem. Sci.* **2017**, *12*, 6180–6189. [CrossRef]
10. Chen, W.; He, Y.; Gao, W. Electrodeposition of sol-enhanced nanostructured Ni-TiO_2 composite coatings. *Surf. Coat. Technol.* **2010**, *204*, 2487–2492. [CrossRef]
11. Allahkaram, S.R.; Golroh, S.; Mohammadalipour, M. Properties of Al_2O_3 nano-particle reinforced copper matrix composite coatings prepared by pulse and direct current electroplating. *Mater. Des.* **2011**, *32*, 4478–4484. [CrossRef]
12. Dai, P.Q.; Zhong, Y.H.; Zhou, X. Corrosion characteristic of pulsed electrodeposition Ni–Co/SiC nanocomposite coating. *Surf. Eng.* **2011**, *27*, 71–76. [CrossRef]
13. Laszczyńska, A.; Winiarski, J.; Szczygieł, B.; Szczygieł, I. Electrodeposition and characterization of Ni–Mo–ZrO_2 composite coatings. *Appl. Surf. Sci.* **2016**, *369*, 224–231. [CrossRef]
14. Tian, B.R.; Cheng, Y.F. Electrolytic deposition of Ni-Co-Al_2O_3 composite coating on pipe steel for corrosion/erosion resistance in oil sand slurry. *Electrochim. Acta* **2007**, *53*, 511–517. [CrossRef]
15. Hammami, O.; Dhouibi, L.; Berçot, P.; Rezrazi, E.M. Zn–Ni/nano-TiO_2 composite electrodeposits: Surface modifications and protective properties. *J. Appl. Electrochem.* **2014**, *44*, 115–121. [CrossRef]
16. Arunsunai Kumar, K.; Paruthimal Kalaignan, G.; Muralidharan, V.S. Direct and pulse current electrodeposition of Ni-W-TiO_2 nanocomposite coatings. *Ceram. Int.* **2013**, *39*, 2827–2834. [CrossRef]
17. Bahrami Mousavi, A.; Baghery, P.; Peikari, M.; Rashed, G. Preparation and characterization of Ni-Cr nanocomposite coatings containing TiO_2 nanoparticles for corrosion protection. *Anti-Corros. Methods Mater.* **2012**, *59*, 279–284. [CrossRef]

18. Gahoi, A.; Wagner, S.; Bablich, A.; Kataria, S.; Passi, V.; Lemme, M.C. Contact resistance study of various metal electrodes with CVD graphene. *Solid State Electron.* **2016**, *125*, 234–239. [CrossRef]
19. Cho, H.K.; Hossain, T.; Bae, J.W.; Adesida, I. Characterization of Pd/Ni/Au ohmic contacts on p-GaN. *Solid State Electron.* **2005**, *49*, 774–778. [CrossRef]
20. Baghery, P.; Farzam, M.; Mousavi, A.B.; Hosseini, M. Ni-TiO_2 nanocomposite coating with high resistance to corrosion and wear. *Surf. Coat. Technol.* **2010**, *204*, 3804–3810. [CrossRef]
21. Wang, Y.; Tay, S.L.; Wei, S.; Xiong, C.; Gao, W.; Shakoor, R.A.; Kahraman, R. Microstructure and properties of sol-enhanced Ni-Co-TiO_2 nano-composite coatings on mild steel. *J. Alloys Compd.* **2015**, *649*, 222–228. [CrossRef]
22. Sangeetha, S.; Paruthimal Kalaignan, G.; Tennis Anthuvan, J. Pulse electrodeposition of self-lubricating Ni-W/PTFE nanocomposite coatings on mild steel surface. *Appl. Surf. Sci.* **2015**, *359*, 412–419. [CrossRef]
23. Sun, Z.; Shen, H.; Wei, X.; Hu, X. Electrocatalytic hydrogenolysis of chlorophenols in aqueous solution on Pd58Ni42 cathode modified with PPy and SDBS. *Chem. Eng. J.* **2014**, *241*, 433–442. [CrossRef]
24. Hosseini, M.G.; Teymorinia, H.; Farzaneh, A.; Khameneh-asl, S. Evaluation of corrosion, mechanical and structural properties of new Ni–W–PCTFE nanocomposite coating. *Surf. Coat. Technol.* **2016**, *298*, 114–120. [CrossRef]
25. Punith Kumar, M.K.; Venkatesha, T.V.; Pavithra, M.K.; Nithyananda Shetty, A. Anticorrosion Performance of Electrochemically Produced Zn-1% Mn-Doped TiO_2 Nanoparticle Composite Coatings. *J. Mater. Eng. Perform.* **2015**, *24*, 1995–2004. [CrossRef]
26. Wang, Y.; Ju, Y.; Wei, S.; Lu, W.; Yan, B.; Gao, W. Mechanical properties and microstructure of Au-Ni-TiO_2 nano-composite coatings. *Mater. Charact.* **2015**, *102*, 189–194. [CrossRef]
27. Chen, X.H.; Chen, C.S.; Xiao, H.N.; Cheng, F.Q.; Zhang, G.; Yi, G.J. Corrosion behavior of carbon nanotubes-Ni composite coating. *Surf. Coat. Technol.* **2005**, *191*, 351–356. [CrossRef]
28. Ranjith, B.; Paruthimal Kalaignan, G. Ni-Co-TiO_2 nanocomposite coating prepared by pulse and pulse reversal methods using acetate bath. *Appl. Surf. Sci.* **2010**, *257*, 42–47. [CrossRef]
29. Guglielmi, N. Kinetics of the Deposition of Inert Particles from Electrolytic Baths. *J. Electrochem. Soc.* **1971**, *119*, 1009–1012. [CrossRef]
30. Grari, O.; Dhouibi, L.; Lallemand, F.; Buron, C.C.; Et Taouil, A.; Hihn, J.Y. Effects of high frequency ultrasound irradiation on incorporation of SiO_2 particles within polypyrrole films. *Ultrason. Sonochem.* **2015**, *22*, 220–226. [CrossRef] [PubMed]
31. Calderón, J.A.; Henao, J.E.; Gómez, M.A. Erosion-corrosion resistance of Ni composite coatings with embedded SiC nanoparticles. *Electrochim. Acta* **2014**, *124*, 190–198. [CrossRef]
32. Sassi, W.; Dhouibi, L.; Berçot, P.; Rezrazi, M.; Triki, E. Study of the electroplating mechanism and physicochemical proprieties of deposited Ni-W-Silicate composite alloy. *Electrochim. Acta* **2014**, *117*, 443–452. [CrossRef]
33. Hou, F.; Wang, W.; Guo, H. Effect of the dispersibility of ZrO_2 nanoparticles in Ni-ZrO_2 electroplated nanocomposite coatings on the mechanical properties of nanocomposite coatings. *Appl. Surf. Sci.* **2006**, *252*, 3812–3817. [CrossRef]
34. Li, Y.; Ives, M.B.; Coley, K.S. Corrosion potential oscillation of stainless steel in concentrated sulphuric acid: I. Electrochemical aspects. *Corros. Sci.* **2006**, *48*, 1560–1570. [CrossRef]
35. Özkan, S.; Hapçi, G.; Orhan, G.; Kazmanli, K. Electrodeposited Ni/SiC nanocomposite coatings and evaluation of wear and corrosion properties. *Surf. Coat. Technol.* **2013**, *232*, 734–741. [CrossRef]
36. Abdel Aal, A. Hard and corrosion resistant nanocomposite coating for Al alloy. *Mater. Sci. Eng. A* **2008**, *474*, 181–187. [CrossRef]
37. Khabazian, S.; Sanjabi, S. The effect of multi-walled carbon nanotube pretreatments on the electrodeposition of Ni-MWCNTs coatings. *Appl. Surf. Sci.* **2011**, *257*, 5850–5856. [CrossRef]
38. Tang, J.; Zhang, Z.; Wang, Y.; Ju, P.; Tang, Y.; Zuo, Y. Corrosion resistance mechanism of palladium film-plated stainless steel in boiling H_2SO_4 solution. *Corros. Sci.* **2018**, *135*, 222–232. [CrossRef]
39. Boissy, C.; Alemany-Dumont, C.; Normand, B. EIS evaluation of steady-state characteristic of 316L stainless steel passive film grown in acidic solution. *Electrochem. Commun.* **2013**, *26*, 10–12. [CrossRef]